ENSO prediction one year in advance using western North Pacific sea surface temperatures

Shih-Yu Wang,[1] Michelle L'Heureux,[2] and Hsin-Hsing Chia[3]

Received 10 January 2012; revised 10 February 2012; accepted 12 February 2012; published 8 March 2012.

[1] We present evidence that the de-trended, boreal winter sea surface temperature anomalies (SSTA) in the western North Pacific (WNP) are a skillful predictor for the development of the El Niño-Southern Oscillation (ENSO) by the following winter. The WNP shares some similarities with the Meridional Mode (MM) located in the subtropical central and eastern North Pacific: both are linked to off-equatorial SSTA and low-level wind anomalies, and both appear to be strongly related to wintertime variability in the North Pacific Oscillation (NPO). However, in contrast with the MM, the WNP is associated with an opposite-signed SSTA dipole located off southeastern Asia and in the western tropical Pacific, which is accompanied by equatorial winds that may influence the level of oceanic Kelvin wave activity that precedes ENSO events. **Citation:** Wang, S.-Y., M. L'Heureux, and H.-H. Chia (2012), ENSO prediction one year in advance using western North Pacific sea surface temperatures, *Geophys. Res. Lett.*, *39*, L05702, doi:10.1029/2012GL050909.

1. Introduction

[2] Previous literature has shown that air-sea interactions between the tropics and higher latitudes can drive variations in ENSO [e.g., *Pierce et al.*, 2000; *Alexander et al.*, 2008]. One possible process is the "Seasonal Footprinting Mechanism (SFM)" popularized by the studies of *Vimont et al.* [2003a, 2003b] and others. It is thought that wintertime variability in the second leading pattern of the atmospheric circulation over the North Pacific, the North Pacific Oscillation (NPO) [*Rogers*, 1981], significantly impacts the sea surface temperature anomalies (SSTA) in the central North Pacific [e.g., *Vimont et al.*, 2009]. The NPO-forced SSTA maximize during the boreal late winter and early spring and potentially excite an atmospheric response that extends deep into the tropical Pacific, impacting ENSO. Previous work strongly suggests that the "Meridional Mode (MM)" index is one of the primary conduits by which the SFM can eventually impact the tropics and ENSO variability [*Chang et al.*, 2007]. The MM index, defined using a Maximum Covariance Analysis (MCA) between SSTA and surface wind anomalies [*Chiang and Vimont*, 2004], is associated with an opposite-signed meridional SSTA gradient located in the central-eastern North Pacific, with one sign of the anomaly maximizing in the subtropics (10–30°N) and the other sign located on the equator. Lag-correlation shows the MM wind index tends to slightly lead the MM SST index, implying the atmospheric circulation is primarily forcing the SSTA pattern. However, coupling is strongly suggested through a "wind-evaporation-SST" feedback [*Chang et al.*, 2007] and by off-equatorial wind stress instigating westward propagating oceanic Rossby waves that reflect back as Kelvin waves and promote the development of ENSO [*Alexander et al.*, 2010]. The MM SST pattern has also been likened to the "optimal structure" of global-scale SSTA, which is a favored pattern that precedes ENSO [*Penland and Sardeshmukh*, 1995].

[3] In this paper, we show that an SSTA dipole in the western North Pacific (WNP) during the boreal winter is related to the development of ENSO by the following winter. The WNP shares characteristics with the MM, except that the meridional SSTA gradient and low-level zonal wind anomalies occur in the western tropical Pacific, which is a key region that determines oceanic Kelvin wave activity prior to ENSO events [*Wyrtki*, 1975; *Giese and Harrison*, 1990; *Vecchi and Harrison*, 2000]. An alternative WNP index can be computed using MCA, but inter-seasonal variations are more simply identified using average de-trended SSTA from 122°–132°E to 18°–28°N centered at the upstream Kuroshio Current east of Taiwan (Figure 1a, yellow box). The advantage of using this WNP index is two-fold: first, it is computationally simple; second, the WNP domain is a busy ship route where in-situ observations are routine and abundant. We utilize two monthly SST datasets: (1) the Hadley Centre SST (HadISST) at a 1° × 1° resolution [*Rayner et al.*, 2003], and (2) the NOAA Extended Reconstructed SST (ERSST) Version 3b at a 2° × 2° resolution [*Smith et al.*, 2008]. The analysis period covers 1958–2010, chosen because of increased observations after the International Geophysical Year. Atmospheric variables are from the NCEP/NCAR Reanalysis [*Kalnay et al.*, 1996].

2. The WNP Index and SSTA Pattern

[4] Figure 1a shows the one-point correlation map of the detrended SSTA with the December-February (DJF) averaged WNP index for several lead times, based on the HadISST data (corresponding plots using ERSSTv3b are shown in Figure S1 in the auxiliary material, which agrees with the HadISST analysis).[1] During DJF, strong correlations are evident near the East Asian coastline (∼20°N) and along the Kuroshio Extension [e.g., *Kwon et al.*, 2010]. Here, the sign of the WNP index is reversed to describe the development El Niño. The linear regression of SSTA and surface winds with the WNP index (Figure 1b, in DJF) depicts northerly and northwesterly flows extending from the East Asian coastline towards the equatorial western Pacific

[1]Department of Plants, Soils, and Climate and Utah Climate Center, Utah State University, Logan, Utah, USA.
[2]Climate Prediction Center, NOAA, Camp Springs, Maryland, USA.
[3]Central Weather Bureau, Taipei, Taiwan.

0094-8276/12/2012GL050909

[1]Auxiliary materials are available in the HTML. doi:10.1029/2011GL050909.

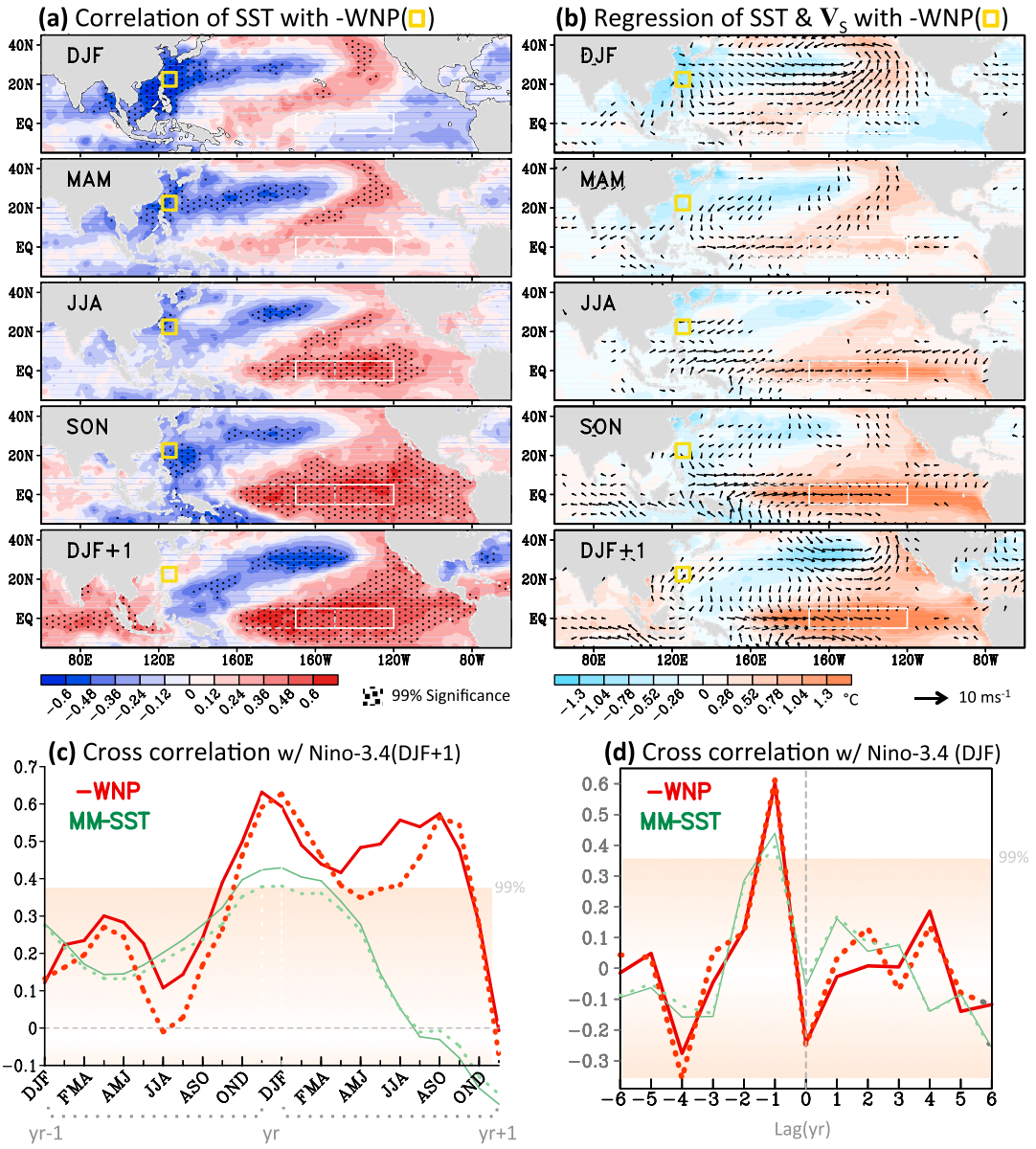

Figure 1. (a) Correlation maps between the December-February (DJF) averaged WNP index and SSTA for DJF and several lead times (MAM, JJA, SON and DJF+1), and (b) corresponding regressions of seasonally averaged SSTA and surface winds onto the DJF averaged WNP index. The WNP (Nino-3.4) domain is outlined in yellow (white). Dotted areas in Figure 1a, vectors in Figure 1b, and shaded areas in Figures 1c and 1d indicate the 99% confidence level. (c) Cross correlations between the DJF+1 averaged Niño-3.4 index and overlapping 3-month averaged values of the WNP (red) and MM-SST (green) indices from year-1 to year+1, and (d) the cross correlation between the lag-0 DJF averaged Niño-3.4 index (in the paper expressed as "DJF+1") and DJF averaged WNP and MM-SST index values computed for 6 year lag to 6 year lead. Here the WNP index is reversed in sign (multiplied by −1). Solid (Dotted) lines represent the HadISST (ERSST) data.

(120°–150°E). Notably, the wind vectors are directed from the below-average SSTs near East Asia toward warmer SSTs in the western equatorial Pacific, and curl eastward along and just north of the equator extending into the central tropical Pacific (140°E–180°). Persistent westerly wind anomalies near the equatorial Pacific are favorable to the development of oceanic Kelvin waves, which can eventually trigger El Niño [e.g., *McPhaden*, 2004]. These westerly wind anomalies strengthen and expand eastward concurrently with the growth of positive SSTA, and El Niño, during the following fall (SON) and winter (DJF+1). Because the analysis is linear, the sign of the anomalies in Figure 1 can be flipped to describe the development leading up to La Niña.

[5] The cross correlation of the moving seasonally averaged WNP index with the Niño-3.4 index of the following winter (DJF+1) is shown in Figure 1c (red line). The peak correlation coefficient occurs in NDJ for HadISST and in DJF for ERSSTv3b. Figure 1d also reveals an oscillatory behavior peaking at a 1-year lag and 4-year lag. This 4-year periodicity is consistent with the dominant timescale of ENSO [e.g., *Zhang et al.*, 2009]. The green line in Figures 1c and 1d show the cross correlation of the DJF+1 Niño-3.4

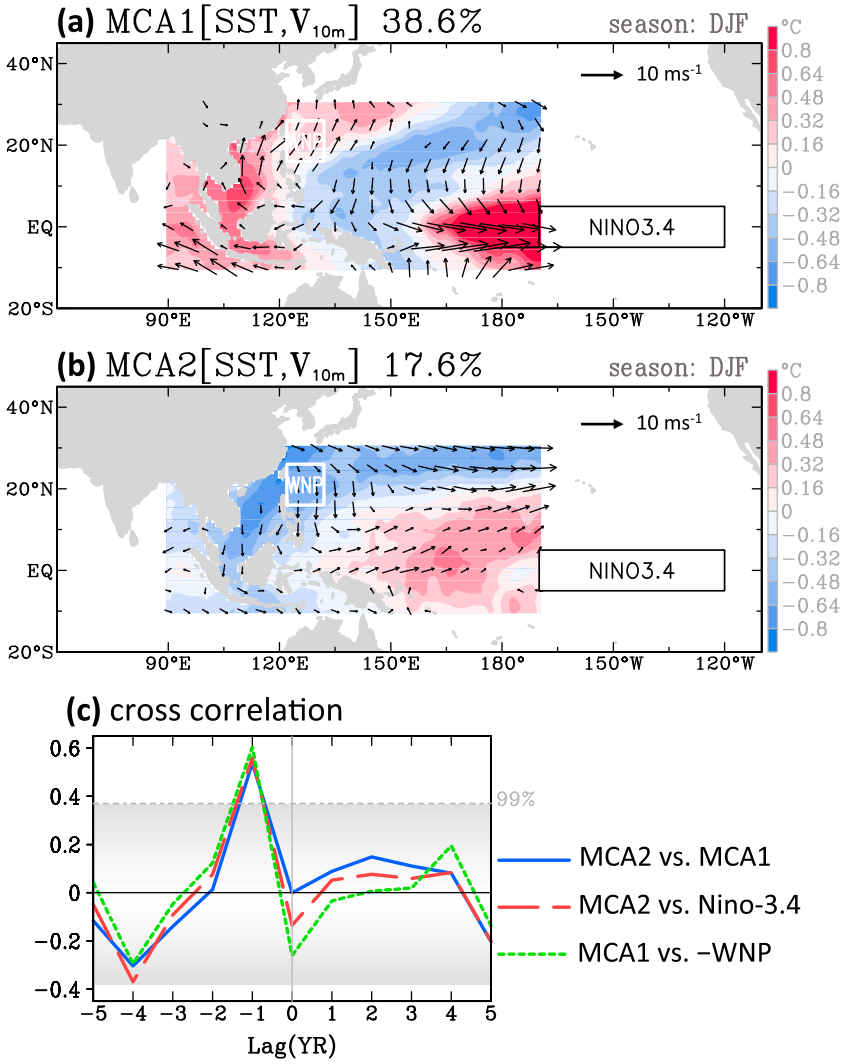

Figure 2. (a) The first and (b) second Maximum Covariance Analysis (MCA) of SSTA (shading) and 10-meter wind anomalies (vectors) during DJF, and (c) cross correlations between i) the leading/lagging DJF averaged values of MCA2 with lag-0 MCA1 (blue line), ii) between the leading/lagging DJF average values of MCA2 and lag-0 Niño-3.4 index (red broken line), and iii) between the DJF averaged MCA1 and inverted WNP index (green dashed line). The WNP and Niño-3.4 domains are outlined in Figures 2a and 2b. Gray shadings in Figure 2c indicate the 99% significance range.

index with seasonally averaged values of the MM index from D. Vimont at http://sunrise.aos.wisc.edu/~dvimont/MModes/Data/. The correlation of the MM-SST index similarly peaks during the winter, but falls short of the peak correlation of the WNP. Also, the WNP correlations with Nino-3.4 persist longer into the year (through SON), while the MM correlations decline significantly after AMJ. Interestingly, the WNP correlations are relatively lower during the boreal spring/early summer, which coincides with the decline of ENSO forecast skill during the so-called "spring barrier," and precedes a secondary peak during the late summer/fall.

[6] Similar to the MM index, we compute the MCA (also known as the Singular Value Decomposition/SVD analysis) for SSTA and 10-meter wind anomalies. However, we focus only on the western Pacific tropical-subtropical domain (90°E–170°W, 10°S–30°N), which excludes the central-eastern Pacific Ocean. As shown in Figure 2a, the first mode of the DJF MCA (explaining 38.6% of the variance) depicts a canonical ENSO structure with alternating signed anomalies in the central tropical Pacific, western tropical Pacific, and South China Sea. This SSTA pattern is accompanied by strong low-level divergence near Papua New Guinea (in the case of El Niño) and it correlates well with the Niño-3.4 index (r = 0.91). The second mode of the DJF MCA (Figure 2b; 17.6% of variance) reveals a pattern similar to the DJF WNP regression in Figure 1b, which precedes El Niño, with below-average SSTs near the eastern and southeastern Asian coastline and above-average SSTs in the western tropical Pacific. Also similar to Figure 1b, the predominantly northerly winds turn to the east along the equator, and flow from colder to warmer SSTs. This second MCA mode is strongly correlated with the WNP index (r = 0.82)[1] and the MM-SST index (r = 0.74) in DJF.

[7] The cross correlation between the coefficients of MCA1 and MCA2 (Figure 2c) is significant (r = 0.6) at 1 year lag, similar to the correlation of MCA2 with the Niño-3.4 index. Also notable at lag-1 is the slightly higher correlation between MCA1 and the WNP index (compared to the other

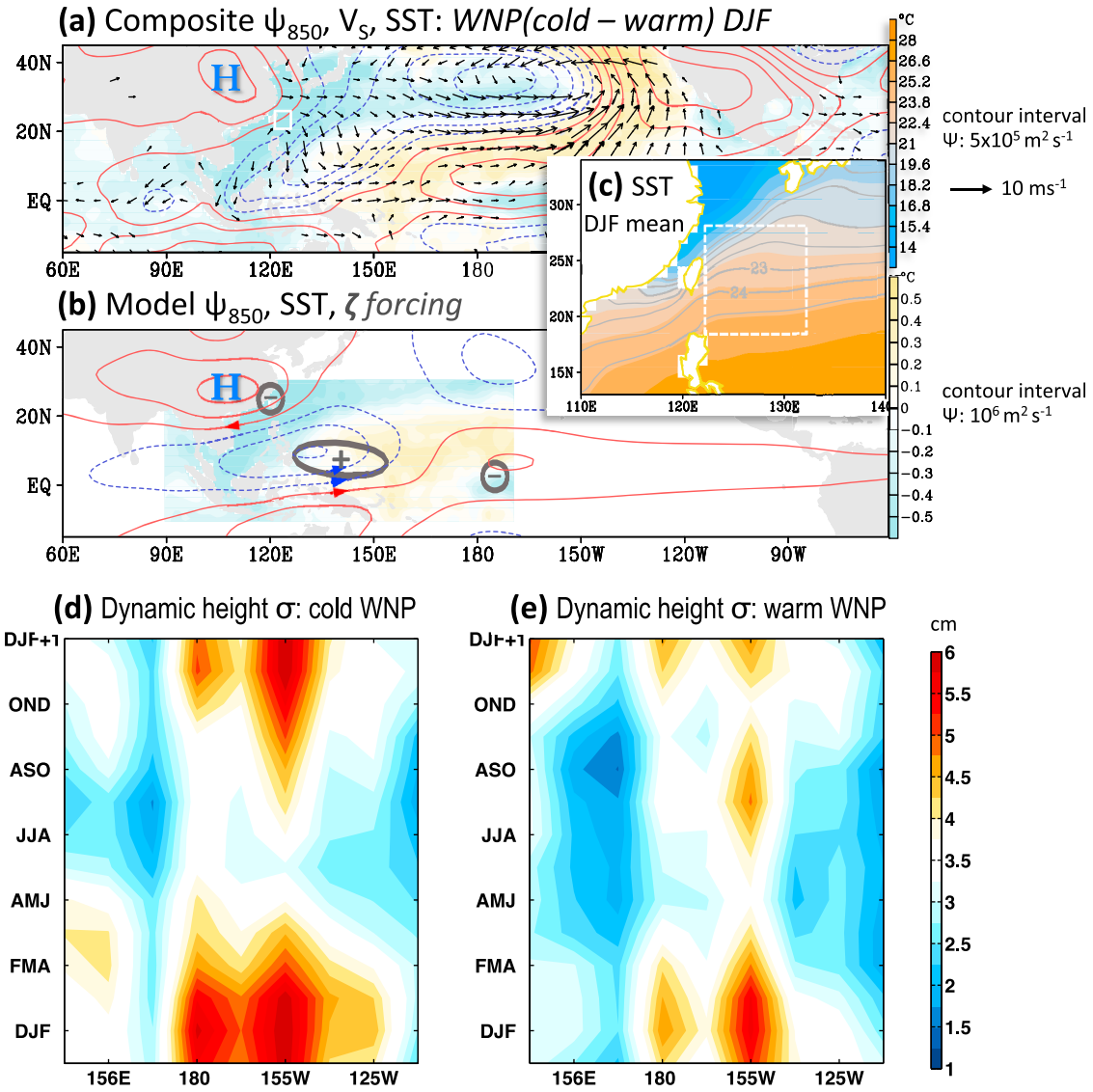

Figure 3. (a) Composite differences of the 850mb streamfunction (contours), SST (shadings) and surface wind vectors between cold WNP index values (1961–63, 65, 68, 70, 77, 80–82, 84, 86, 87, 89, 90, 92, 96, 97, 06, 08, 09) and warm WNP index values (1958–60, 66, 71–73, 75, 83, 88, 98–01, 07) during winters centered in January (DJF) (|SSTA|>0.15°C). (b) The 850mb eddy streamfunction response (contours) to the three vorticity forcing sources (thick gray outlines) simulated from the barotropic model, superimposed with the composite SSTA within the MCA domain (shadings). (c) Climatological SSTs in DJF; the WNP domain is outlined in white. (d) Standard deviation of the oceanic Kelvin wave dynamic height anomalies during NDJ averaged cold WNP winters and subsequent seasons out to DJF+1. (e) Same as Figure 3d but for NDJ averaged warm WNP winters.

two index pairs), as well as the significant correlation at lag-4 between MCA2 and the Niño-3.4 index. More importantly, MCA2 demonstrates that the WNP index is reflecting the same large-scale pattern of low-level winds corresponding to a northwest-southeast SSTA dipole in the tropical and subtropical western Pacific.

3. Possible Mechanisms

[8] To diagnose the potential influence of the SSTA onto the atmospheric circulation anomalies, we construct composites and compare them to a linear barotropic model [e.g., *Branstator*, 1985]. For comparison, a composite difference (cold – warm WNP) of the 850mb streamfunction, surface winds, and SSTA for DJF are shown in Figure 3a. Figure 3b shows the result of the model simulation, which is created by inserting a positive vorticity source east of the Philippines ("+" in Figure 3b) sandwiched by two negative sources ("–"). These three vorticity source regions were determined using composite precipitation anomalies (not shown) and tend to occur at the nodes of the SSTA pattern. The areas of vorticity forcing (with a prescribed value of 10^{-5} s^{-1}) are used to perturb the barotropic model, using the winter mean 850mb streamfunction as the basic state. As shown in Figure 3b, the simulated streamfunction anomalies depict a Gill-type response with a pair of low-level cyclonic

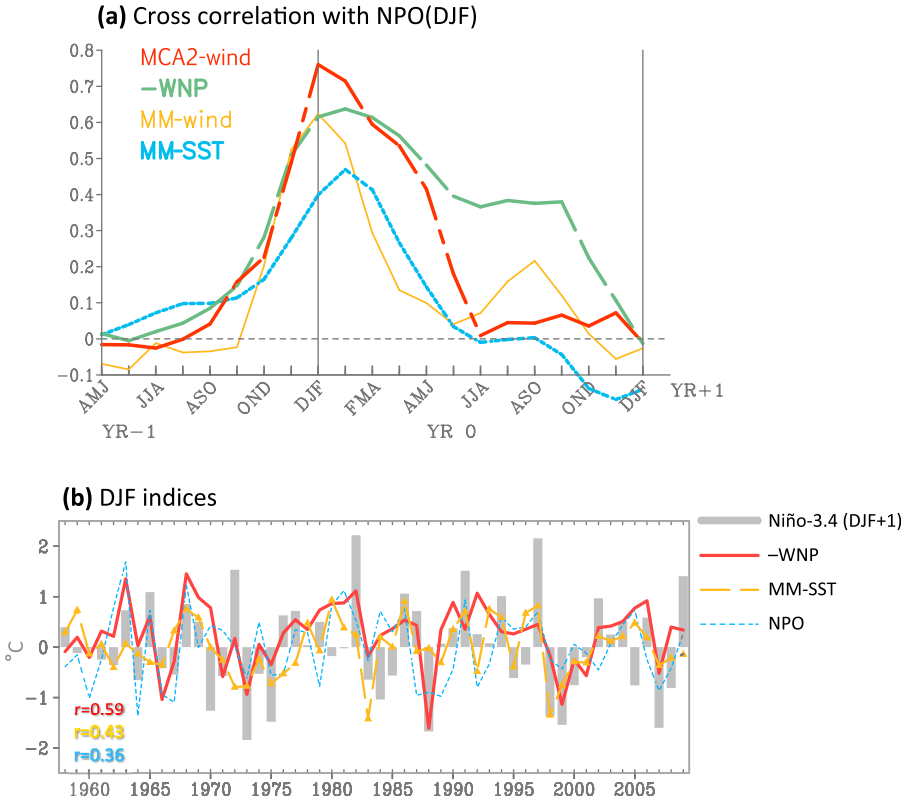

Figure 4. (a) Cross correlations between the DJF averaged NPO index and overlapping 3-month averaged values of the MCA2-wind (red), inverted WNP (green), MM-wind (golden) and MM-SST (cyan) indices. (b) DJF averaged time series of the inverted WNP (red), MM-SST (golden) and NPO (cyan) indices overlaid with the Niño-3.4 index in DJF+1 (gray bars). Except for Niño-3.4, all indices are standardized and multiplied by two; their correlations are displayed at the lower left corner. The Niño-3.4 and WNP indices are derived from the HadISST data.

anomalies straddling the equator west of positive equatorial SSTA and two anticyclonic anomalies to the east. A Rossby wave train is implied by the anticyclonic anomaly located over East Asia (indicated by "H" in Figure 3a).

[9] Despite the crudeness of this diagnostic simulation, as it lacks any mid-latitude forcing and air-sea feedback, the overall similarity with observations supports the idea that the SSTA dipole associated with the WNP may affect the East Asian winter monsoon. *Li* [1990] found that anomalously cold winters over eastern China often preceded El Niño events by a year. Although not tested here, it is conceivable that flow from the anomalous East Asian anticyclone could feedback onto the initial SSTA, enhancing cold air advection over the Kuroshio Current region (Figure 3c) and further cooling the SSTs (as in cold WNP cases). Likewise, a cyclonic anomaly may result in warm air advection towards the East Asian coastal seas and consequently warm the SSTs (during warm WNP cases). The WNP domain (Figure 3c) is situated in an optimal position, i.e., over the strong SST gradients, to capture such wind-SST relationships associated with the East Asian winter monsoon.

[10] From the observations and model simulation, it is clear that the WNP-related wintertime circulation anomalies favor wind anomalies over the equatorial western Pacific. The occurrence of low-level westerlies imparts a stress on the ocean surface that often triggers oceanic Kelvin waves that propagate eastward and help initiate El Niño events [e.g., *Roundy and Kiladis*, 2006]. *Roundy* [2007] reconstructed daily ocean dynamic height departures from 1974–2005 using the TAO buoys and the sea level time series for 11 stations, and filtered them (20–120 days) to identify oceanic Kelvin waves. Using this data, composites were constructed using the years associated with NDJ cold WNP events out to a year, which is consistent with the build-up prior to ENSO [e.g., *Seo and Xue*, 2005]. In each category, the standard deviation was computed for all days within the seasonal average at each longitude. The resulting analysis shows that the standard deviation of dynamic heights is considerably larger for cold WNP events than the warm WNP events. Possibly, the cold WNP winters, with enhanced low-level westerly wind anomalies, contribute to higher oceanic Kelvin wave activity that persists through the following winter (consistent with El Niño). Conversely, the enhancement of easterly trade winds in the equatorial Pacific, following warm WNP winters, suppresses oceanic Kelvin wave activity into the following winter (consistent with La Niña).

4. Discussions and Future Work

[11] Previous work indicates that wintertime NPO variability influences ENSO the following year through the SFM. Because the MM pattern is often considered a conduit for the NPO to eventually influence ENSO, it is worth comparing the relationship between the WNP and the NPO. Figure 4a shows the cross correlations of the DJF average NPO index

(projection onto the 2nd Principal Component of Nov-Mar 1000-hPa height anomalies for 20–90°N to 120°E–120°W) with moving seasonal averages of the WNP index, the MCA-2 index for 10-m wind anomalies across the western Pacific domain shown in Figure 2b ("MCA2-wind"), the MM wind index, and the MM SST index. It is evident that both western North Pacific indices (WNP and MCA2-wind) exceed the correlations associated with the MM indices. Moreover, as in Figure 1c, it is clear that both the MCA2-wind and the WNP indices have a longer staying power through the year than the MM. Figure 4b shows the time-series of Niño-3.4 (DJF+1) index (in °C) alongside the DJF averaged WNP index, the MM-SST index, and the NPO index. The correlations of each of these indices with the following winter Nino-3.4 index are shown in the lower left corner.

[12] From Figure 4, it is apparent that while wintertime NPO variability is strongly related to both the MM pattern and the WNP pattern, the WNP may act as an improved conduit between the mid-latitude atmospheric variability and ENSO the following winter. We argue that because of its location, the WNP-associated SST dipole and wind anomalies contribute more directly to oceanic Kelvin wave activity in the western tropical Pacific that precedes ENSO events. Future work should further examine to what extent the East Asian winter monsoon [e.g., *Kim and Lau*, 2001] and variability in the Kuroshio Current sets the stage for ENSO the following winter.

[13] Previous work related to the SFM has largely emphasized the role of SSTA in the central-eastern North Pacific as a precursor to ENSO. This work is fundamental to understanding how mid-latitude variability can impact ENSO and it is likely that the off-equatorial SSTA linked to the MM and WNP are strongly interconnected during the development of ENSO. However, it is worth investigating the relative contribution of each region to the development of ENSO and further understanding to what extent the NPO → WNP → ENSO process can occur independent of variability in the central-eastern North Pacific.

[14] **Acknowledgments.** We appreciate valuable comments on the initial manuscript by Michael Alexander, Zeng-Zhen Hu, and Wanqiu Wang. We also thank Dan Vimont for providing the MM index and Paul Roundy for providing the reconstructed dynamic height data. This study was supported partially by the Utah Agricultural Experiment Station, Utah State University, under paper 8393 and by grant MOTC-CWB-101-M-15.

[15] The Editor thanks two anonymous reviewers for their assistance in evaluating this paper.

References

Alexander, M. A., et al. (2008), Forecasting Pacific SSTs: Linear inverse model predictions of the PDO, *J. Clim.*, *21*, 385–402, doi:10.1175/2007JCLI1849.1.

Alexander, M. A., D. J. Vimont, P. Chang, and J. D. Scott (2010), TheiImpact of extratropical atmospheric variability on ENSO: Testing the seasonal footprinting mechanism using coupled model experiments, *J. Clim.*, *23*, 2885–2901, doi:10.1175/2010JCLI3205.1.

Branstator, G. (1985), Analysis of general circulation model sea-surface temperature anomaly simulations using a linear model. Part I: Forced solutions, *J. Atmos. Sci.*, *42*, 2225–2241, doi:10.1175/1520-0469(1985)042<2225:AOGCMS>2.0.CO;2.

Chang, P., L. Zhang, R. Saravanan, D. J. Vimont, J. C. H. Chiang, L. Ji, H. Seidel, and M. K. Tippett (2007), Pacific meridional mode and El Niño–Southern Oscillation, *Geophys. Res. Lett.*, *34*, L16608, doi:10.1029/2007GL030302.

Chiang, J. C. H., and D. J. Vimont (2004), Analogous Pacific and Atlantic meridional modes of tropical atmosphere–ocean variability, *J. Clim.*, *17*, 4143–4158, doi:10.1175/JCLI4953.1.

Giese, B. S., and D. E. Harrison (1990), Aspects of the Kelvin wave response to episodic wind forcing, *J. Geophys. Res.*, *95*, 7289–7312, doi:10.1029/JC095iC05p07289.

Kalnay, E., et al. (1996), The NCEP/NCAR 40-year reanalysis project, *Bull. Am. Meteorol. Soc.*, *77*, 437–471, doi:10.1175/1520-0477(1996)077<0437:TNYRP>2.0.CO;2.

Kim, K.-M., and K.-M. Lau (2001), Dynamics of monsoon-induced biennial variability in ENSO, *Geophys. Res. Lett.*, *28*(2), 315–318, doi:10.1029/2000GL012465.

Kwon, Y.-O., M. A. Alexander, N. A. Bond, C. Frankignoul, H. Nakamura, B. Qiu, and L. A. Thompson (2010), Role of the Gulf Stream and Kuroshio-Oyashio systems in large-scale atmosphere–ocean interaction: A review, *J. Clim.*, *23*, 3249–3281, doi:10.1175/2010JCLI3343.1.

Li, C. (1990), Interaction between anomalous winter monsoon in East Asia and El Niño events, *Adv. Atmos. Sci.*, *7*, 36–46, doi:10.1007/BF02919166.

McPhaden, M. J. (2004), Evolution of the 2002/03 El Niño, *Bull. Am. Meteorol. Soc.*, *85*, 677–695, doi:10.1175/BAMS-85-5-677.

Penland, C., and P. D. Sardeshmukh (1995), The optimal growth of tropical sea surface temperature anomalies, *J. Clim.*, *8*, 1999–2024, doi:10.1175/1520-0442(1995)008<1999:TOGOTS>2.0.CO;2.

Pierce, D. W., T. P. Barnett, and M. Latif (2000), Connections between the Pacific Ocean tropics and midlatitudes on decadal timescales, *J. Clim.*, *13*, 1173–1194, doi:10.1175/1520-0442(2000)013<1173:CBTPOT>2.0.CO;2.

Rayner, N. A., D. E. Parker, E. B. Horton, C. K. Folland, L. V. Alexander, D. P. Rowell, E. C. Kent, and A. Kaplan (2003), Global analyses of sea surface temperature, sea ice, and night marine air temperature since the late nineteenth century, *J. Geophys. Res.*, *108*(D14), 4407, doi:10.1029/2002JD002670.

Rogers, J. C. (1981), The North Pacific Oscillation, *J. Climatol.*, *1*, 39–57, doi:10.1002/joc.3370010106.

Roundy, P. E. (2007), Analysis of a reconstructed oceanic Kelvin wave dynamic height dataset for the period 1974–2005, *J. Clim.*, *20*, 4341–4355, doi:10.1175/JCLI4249.1.

Roundy, P. E., and G. N. Kiladis (2006), Observed relationships between oceanic Kelvin waves and atmospheric forcing, *J. Clim.*, *19*, 5253–5272, doi:10.1175/JCLI3893.1.

Seo, K.-H., and Y. Xue (2005), MJO-related oceanic Kelvin waves and the ENSO cycle: A study with the NCEP Global Ocean Data Assimilation System, *Geophys. Res. Lett.*, *32*, L07712, doi:10.1029/2005GL022511.

Smith, T. M., R. W. Reynolds, T. C. Peterson, and J. Lawrimore (2008), Improvements to NOAA's Historical Merged Land–Ocean Surface Temperature Analysis (1880–2006), *J. Clim.*, *21*, 2283–2296, doi:10.1175/2007JCLI2100.1.

Vecchi, G. A., and D. E. Harrison (2000), Tropical Pacific sea surface temperature anomalies, El Niño, and equatorial westerly wind events, *J. Clim.*, *13*, 1814–1830, doi:10.1175/1520-0442(2000)013<1814:TPSSTA>2.0.CO;2.

Vimont, D. J., J. M. Wallace, and D. S. Battisti (2003a), The seasonal footprinting mechanism in the Pacific: Implications for ENSO, *J. Clim.*, *16*, 2668–2675, doi:10.1175/1520-0442(2003)016<2668:TSFMIT>2.0.CO;2.

Vimont, D. J., D. S. Battisti, and A. C. Hirst (2003b), The seasonal footprinting mechanism in the CSIRO general circulation models, *J. Clim.*, *16*, 2653–2667, doi:10.1175/1520-0442(2003)016<2653:TSFMIT>2.0.CO;2.

Vimont, D. J., M. Alexander, and A. Fontaine (2009), Midlatitude excitation of tropical variability in the Pacific: The role of thermodynamic coupling and seasonality, *J. Clim.*, *22*, 518–534, doi:10.1175/2008JCLI2220.1.

Wyrtki, K. (1975), El Niño—The dynamic response of the equatorial Pacific Ocean to atmospheric forcing, *J. Phys. Oceanogr.*, *5*, 572–584, doi:10.1175/1520-0485(1975)005<0572:ENTDRO>2.0.CO;2.

Zhang, L., P. Chang, and L. Ji (2009), Linking the Pacific meridional mode to ENSO: Coupled model analysis, *J. Clim.*, *22*, 3488–3505, doi:10.1175/2008JCLI2473.1.

H.-H. Chia, Central Weather Bureau, 64, Kung-Yuan Rd., Taipei 100, Taiwan.

M. L'Heureux, Climate Prediction Center, NOAA, 5200 Auth Rd., Camp Springs, MD 20746, USA.

S.-Y. Wang, Department of Plants, Soils, and Climate, Utah State University, 4820 Old Main Hill, Logan, UT 84322, USA. (simon.wang@usu.edu)